ChemComm

Accepted Manuscript

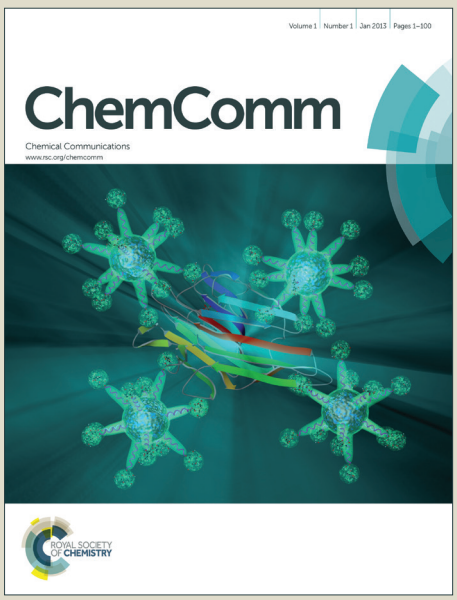

ROYAL SOCIETY OF CHEMISTRY

www.rsc.org/chemcomm

Journal Name

RSCPublishing

COMMUNICATION

Gas-liquid interface-mediated room-temperature synthesis of "clean" PdNiP alloy nanoparticle networks with high catalytic activity for ethanol oxidation

Cite this: DOI: 10.1039/x0xx00000x

Received ooth January 2012,
Accepted ooth January 2012

DOI: 10.1039/x0xx00000x

www.rsc.org/

Rongfang Wang,[a*] Yuanyuan Ma,[a] Hui Wang,[a] Julian Key[b] and Shan Ji[b]

PdNiP alloy nanoparticle networks (PdNiP NN) were prepared by simultaneous reduction of $PdCl_2$, $NiCl_2$ and NaH_2PO_2 with $NaBH_4$ via a gas-liquid interface reaction at room temperature using N_2 bubbles. PdNiP NN had markedly higher activity and durability for ethanol oxidation than PdNi nanoparticle networks and PdNiP grain aggregates.

Noble metal-based alloys are well known for their excellent electrocatalytic performance as fuel cell oxidation catalysts of small organic molecules. Various factors such as their morphology, composition and nano-structural architecture can contribute to their catalytic performance[1]. In particular, porous or network structures are of great interest due to their high surface area-to-volume ratio, low density, and high gas permeability compared to their solid counterparts[2]. Such structures are often synthesized by either hard template synthesis or chemical/electrochemical dealloying from a binary or multicomponent alloy[3-5]. However, these methods are expensive due to their sacrificial components. Similarly, PtNi and PtCo alloy networks have been prepared by reducing metal precursors with NaBH4 in water using a soft surfactant template of cetyltrimethylammonium bromide (CTAB)[6,7]. These catalysts had high methanol oxidation activity and high oxygen reduction activity respectively. However, reports also show that effective removal of adsorbed surfactant from the surface of metals or alloys, to obtain a "clean" surface, can be a difficult process[8]. In addition, despite considerable investigation of Pt-based alloy networks, relatively few works have explored Pd-based alloy networks. Recently, Lu et al. prepared PdCoP alloy networks by reducing $K_2PdCl_4/K_3Co(CN)_6$ cyanogel without any surfactants[9], but the precursor, $K_3Co(CN)_6$, is strongly toxic. Therefore, the search for facile, green, low-cost and universal synthetic processes for making "clean" porous or network-like nanomaterials appears to remain challenging.

Interfacial interactions can be used for guided growth of various nanostructures. Li's research group successfully synthesized MSe (M=Mn, Ni and Co) nanocrystals using a gas-liquid interface reaction method[10]. Such results suggest that the approach could be used to synthesize network-like alloys with clean surfaces. Herein, we present a facile room-temperature reaction to form "clean" PdNiP networks at a gas-liquid interface. We chose the PdNiP composite for two reasons. Firstly, PdNi has excellent catalytic activity for ethanol oxidation reaction (EOR) in alkaline electrolyte[11]. Secondly, the addition of P can enhance the activity of metal or alloys such as Pd[12],PdP[13], PtRu[14], PtNi[1,15], and PdNi[16] for small organic molecule oxidation due to synergistic effects between metal/alloys and P. In correlation, the herein-prepared PdNiP alloy nanoparticle network (PdNiP NN) had high catalytic activity for EOR in alkaline medium. Moreover, our method allowed both the preparation of network-like alloys such as PdCoP NN and PdNi NN as well as PdNiP NN nanoparticle networks with adjustable composition.

PdNiP NN was synthesized by co-reduction of $PdCl_2$, $NiCl_2$, and NaH_2PO_2 with $NaBH_4$ in water bubbled with N_2 at room temperature (see ESI for details). Fig. 1a and 1b show low and high magnification scanning electron microscopy (SEM) images of PdNiP-1 NN respectively. PdNiP-1 NN clearly comprised an extensive network-like structure of sub-10 nm aligned nanoparticles, which was also visible using transmission electron microscopy (TEM) (Fig. 1c). High resolution TEM further showed that most particles had elliptical morphology of 2–9 nm diameter (Figure 1d). Visible lattice fringes and selected area electron diffraction (SAED) pattern (inset Fig. 1d) indicate the PdNiP-1 NN alloy had crystalline state. Figure 1e shows the distribution profile of elements P, Ni and Pd in a typical region (i.e. the red bar across the STEM image inset). On the whole, the positions and widths of the peaks of the three elements matched with each other, indicating PdNiP-1 NN had uniform distribution of the three elements. Using ICP analysis (Table S1) the atomic ratio of Pd:Ni:P in the bulk composition of PdNiP NN was 1:5.2:11.

XRD analysis of PdNiP-1 NN and PdNi NN (Fig. 1f) revealed diffraction peaks at 39.4, 45.4, 67.1, and 81.0 correlate to (111), (200),

(220), and (311) diffractions respectively, which fit the typical pattern of polycrystalline Pd face-centered cubic (fcc) phase (JCPDS 89-4897:

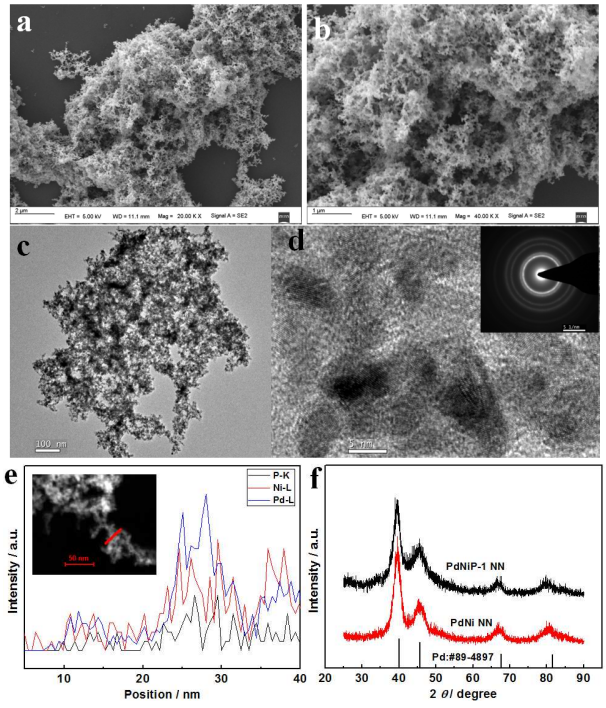

Fig. 1. (a,b) SEM images of PdNiP-1 NN at different magnifications. (c,d) TEM and HRTEM images of PdNiP-1 NN. The inset shows the SAED pattern of PdNiP-1 NN. (e) Line-scan EDS profile of PdNiP-1 NN. The inset shows the STEM image of PdNiP-1 NN. (f) XRD patterns of PdNiP-1 NN and PdNi NN.

marked with the solid black vertical lines). The diffraction peaks of PdNi NN shifted to a slightly higher 2θ degree compared to pure Pd, implying that the lattice parameter had shrunk. Most likely, some Pd atoms were displaced by the smaller Ni atoms, leading to the smaller lattice parameter of PdNi NN. In contrast, the peaks of PdNiP-1 NN shifted negatively, indicating an expansion of the Pd lattice due to incorporation of P atoms, a phenomenon previously observed for PdNiP/C[16].

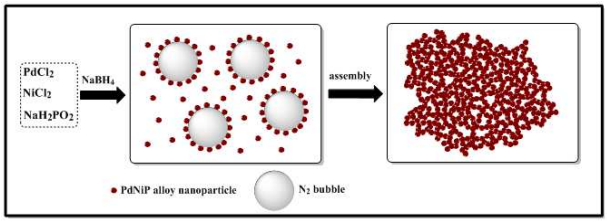

Scheme 1. Schematic process of PdNiP NN formation on N_2 bubbles.

To determine the importance of N_2 bubbles during PdNiP NN formation, a control experiment in the absence of N_2 bubbles was carried out. Here, PdNiP grain aggregates (PdNiP GA) were formed instead of a network structure (ESI, Fig. S1). Therefore, we hypothesize, according to a proposed "gas-liquid interface aggregation mechanism"[10], that N_2 bubbles provide nucleation sites for PdNiP particle aggregation, and once the concentration of PdNiP nanoparticles on the interface region is sufficiently high, the nanoparticles assemble to form a network structure (Scheme 1). As such, the N_2 bubbles appear to act as a soft template for obtaining network structure. A control experiment was completed in the preparation of the PdNiP NN material so as to elucidate the role of the N2 bubbling gas in the formation of the porous solid. An inert gas, Argon, was used in place of N2 so as to determine if the chemical affinity of the bubbling gas played a role in the formation of the nanoparticle network. Fig. S2 shows no difference in the nanoparticle formed from either N2 or Ar. On extending the method to synthesis of PdNi, and PdCoP, nanoparticle network structures were also successfully formed for these alloys (Fig. S3 and 4 (ESI)).

It is well established that multimetallic alloy electrocatalysts have composition-dependent activities. Previous reports on PdNi alloys have extensively investigated the effect of the Pd:Ni molar ratio on ethanol oxidation activity[17]. Here, we considered the effect of the amount of P in PdNiP NN on the catalytic performance. Then, PdNiP NN with different composition, PdNiP-2 and PdNiP-3 NN, could be successfully synthesized by adjusting the molar ratio of metal precusors, as shown in Fig. S5 and 6(ESI). Thus, it is justifiable to expect that modulating P ratio in PdNiP NN could help to design and synthesize catalysts with superior catalytic activities.

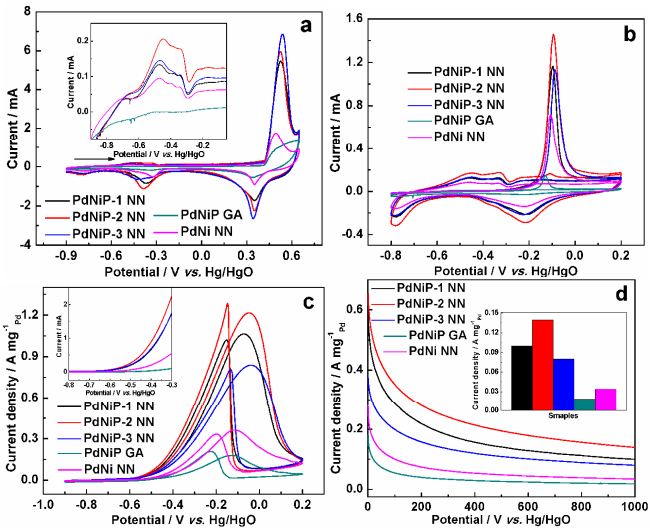

Fig. 2. (a) CVs on PdNiP NN, PdNiP GA and PdNi NN electrodes, the inset shows an enlargement of the forward scan between 0.9 V and -0.05 V; Solution: N_2-saturated 1.0 mol L^{-1} KOH, scan rate: 50 mV s^{-1}. (b) CO stripping voltammetry on PdNiP NN, PdNiP GA and PdNi NN electrodes in N_2-saturated 1.0 mol L^{-1} KOH solution at a scan rate of 50 mV s^{-1}. (c) EOR CVs on PdNiP NN, PdNiP GA and PdNi NN electrodes at a scan rate of 50 mV s^{-1}; The inset shows LSV on PdNiP NN, PdNiP GA and PdNi NN electrodes a scan rate of 5 mV s^{-1}; Solution: N_2-saturated 1.0 mol L^{-1} C_2H_5OH + 1.0 mol L^{-1} KOH. (d) Chronoamperometry curves on PdNiP NN, PdNiP GA and PdNi NN electrodes in N_2-saturated 1.0 mol L^{-1} C_2H_5OH + 1.0 mol L^{-1} KOH solution at a fixed potential of -0.3 V *vs.* Hg/HgO. The inset shows the current density on the all electrodes at 1000 s.

Cyclic voltammetry was first carried out on PdNiP NN, PdNiP GA and PdNi NN electrodes over a wide voltage range to evaluate the electrochemical behavior of the materials in the absence of ethanol (Figure 2a). All three materials produced a weak broad peak in the forward scan between -0.69 and -0.29 V (enlarged in the inset), which was likely due to OH^- adsorption on the surface of the catalysts[19]. The strong oxidation peak at ~0.53 V correlates to $Ni(OH)_2$ oxidation to NiOOH. On the reverse sweep, the defined peak near 0.35 V was characteristic of the reduction of NiOOH to $Ni(OH)_2$, and was followed

by the reduction peak of PdO to Pd at around -0.38 V. The results suggest that both Pd and Ni were present in all three catalysts.

Here, ECSAs were evaluted by the charge of the oxidation region of CO (Figure 2b) on the electrodes due to the penetration of hydrogen into the Pd-based metallic structures. ECSA values listed in Table S2 (EIS) of the materials increased via the following trend: PdNiP GA < PdNi NN < PdNiP-3 NN < PdNiP-1 NN < PdNiP-2 NN. This implies PdNiP NN would provide more active sites for catalysis than PdNiP GA and PdNi NN. In addition, the onset potential of CO is in the order of PdNiP GA > PdNi NN ≈ PdNiP-3 > PdNiP-1 ≈PdNiP-2 NN, demonstrating that, in being more negative, PdNiP NN have better CO catalytic activity than PdNiP GA and PdNi NN.

Fig. 2c shows the EOR CVs of the three catalysts, and the current was normalized to the Pd mass on the electrodes. The value of peak current was listed in Table S2 (EIS). Among three PdNiP NN catalysts, PdNiP-2 NN produced the highest EOR catalytic activity in terms of peak current density, indicating that the optimal P ratio with the highest mass activity was 1:5:8 of Pd:Ni:P. The peak current density for EOR on PdNiP-2 NN electrode was 6.6 and 3.3 fold that of PdNiP GA and PdNi respectively. Effective EOR catalysts have low EOR onset potentials. The inset in Fig. 2c shows the EOR onset potentials measured by linear scan voltammetry (LSV) on PdNiP NN, PdNiP GA, and PdNi NN catalysts. PdNiP-2 NN produced the lowest onset potential (-0.706 V) among the five catalysts, which was 163 and 73 mV more negative than that of PdNiP GA (-0.549 V) and PdNi NN (-0.639 V) respectively. Regarding both mass activity and EOR onset potential, PdNiP NN has higher catalytic activity than PdNiP GA and PdNi NN. In addition, compared to the activity of other reported catalysts[17-19] showed in Table S2(EIS), PdNiP-2 NN also has good EOR catalytic activity in terms of the onset potential or the peak mass activity. To determine the origin of enhanced EOR catalytic on PdNiP-2 NN, the surface area by Brunauer -Emmett-Teller (BET) method and X-ray photoelectron spectra (XPS) were provided in Fig. S7-10 and Table S3-4. As we can see, PdNiP-2 has larger BET surface area than PdNiP GA and PdNi NN, which would provide large contact area for catalytsis. On the other hand, from Fig. S8 and Table S4, the binding energy of Pd 3d in PdNiP-2 NN and PdNiP GA negatively shifts ca. 0.3 eV related to that of PdNi NN, indicating that the electronic structure of Pd is modifiy by the P atoms. Based on these results, the high surface area and the electronic effect between Pd, Ni and P enhanced the activity of PdNiP NN for EOR.

Fig. 2d shows the mass activity-time plots of three materials after 1000 s (summarized in the inset). As expected, PdNiP-2 NN produced the highest EOR oxidation current density at 1000 s, i.e., 0.14 A mg^{-1}_{Pd}, which was 7.8 and 4.1 times higher than on PdNiP GA (0.018 A mg^{-1}_{Pd}) and PdNi NN (0.034 A mg^{-1}_{Pd}) respectively. This result corresponds well with the CO stripping voltammetry and CVs of EOR results.

Finally, the stability of PdNiP-2 NN for EOR was also studied. As indicated by the CVs shown in Fig. S11, PdNiP-2 NN loses nearly 31.6% of its mass activity after about 400 cycles of potential cycling. Compared to the work of Zhang's group[6], the stability of PdNiP-2 NN is poor. By comparison of change of morphology (Fig. S11) and composition (ESI) before and after cycles, the decrease activity is mainly related to the leaching of P in PdNiP-2 NN.

In summary, a PdNiP alloy with nanoparticle network structure (PdNiP NN) was fabricated by an N_2 gas-liquid interface reaction at room temperature. N_2 bubbles acted as a soft template during the simultaneous reduction of precursors containing Pd, Ni and P. The as-prepared PdNiP NN material produced higher EOR activity (i.e. a higher mass activity and lower onset potential) and better durability than both PdNiP GA and PdNi NN. Optimum EOR performance on PdNiP was achieved using a 1:5:8 atomic ratio composition of Pd:Ni:P. Overall, PdNiP NN appears to be a promising EOR catalyst for direct ethanol fuel cells, and the synthesis method offers a facile means to produce "clean", high-activity, nanoparticle network alloy catalysts of controllable composition.

This work was financially supported by the National Science Foundation of China (Grant No. 21163018, 21363022, and 51362027).

Notes and references

[a]*Key Laboratory of Eco-Environment-Related Polymer Materials, Ministry of Education of China,* College of Chemistry and Chemical Engineering, Northwest Normal University, Lanzhou 730070, China Email: wangrf@nwnu.edu.cn, fax/Tel.:+86 931 7971533

[b]South African Institute for Advanced Materials Chemistry, University of the Western Cape, Cape Town 7535, South Africa

Electronic Supplementary Information (ESI) available: [details of experimental, SEM images, BET, XPS and electrochemical performance of PdNiP-2 and PdNiP-3]. See DOI: 10.1039/c000000x/

1. Y. Ma, R. Wang, H. Wang, V. Linkov and S. Ji, *Phys.Chem. Chem. Phys.* 2014, **16**, 3593-3602.
2. J. Yu, Y. Ding, C. Xu, A. Inoue, T. Sakurai and M. Chen, *Chem. Mater.*, 2008, **20**, 4548-4550.
3. W. Wang, R. Wang, H. Wang, S. Ji, J. Key, X. Li and Z. Lei, *J. Power Sources*, 2011, **196**, 9346-9351.
4. W. Wang, S. Ji, H. Wang and R. Wang, *Fuel Cells*, 2012, **12**, 1129-1133.
5. B. C. Tappan, S. A. Steiner and E. P. Luther, *Angew. Chem. Int. Ed.*, 2010, **49**, 4544-4565.
6. Y. Xu, Y. Yuan, A. Ma, X. Wu, Y. Liu and B. Zhang, *ChemPhysChem* 2012, **13**, 2601-2609.
7. Y. Xu, S. Hou, Y. Liu, Y. Zhang, H. Wang and B. Zhang, *Chem. Commun.*, 2012, **48**, 2665-2667.
8. J. Wang, X.B. Zhang, Z.-L. Wang, L.-M. Wang, W. Xing and X. Liu, *Nanoscale*, 2012, **4**, 1549-1552.
9. L. Zhang, D. Lu, Y. Chen, Y. Tang and T. Lu, *J. Mater. Chem. A*, 2014, **2**, 1252-1256.
10. X. Wang, Q. Peng and Y. Li, *Acc. Chem. Res.*, 2007, **40**, 635-643.
11. T. Ramulifho, K. I. Ozoemena, R. M. Modibedi, C. J. Jafta and M. K. Mathe, *Electrochim. Acta*, 2012, **59**, 310-320.
12. G. Yang, Y. Chen, Y. Zhou, Y. Tang and T. Lu, *Electrochem. Commun.*, 2010, **12**, 492-495.
13. J. Zhang, Y. Xu, B. Zhang, *Chem. Commun.* 2014, DOI:10.1039/c4cc0328a.
14. J. Xie and D. G. Xia, *Fuel Cells*, 2013, **13**, 143-148.
15. L. X. Ding, A. L. Wang, G. R. Li, Z. Q. Liu, W. X. Zhao, C. Y. Su and Y. X. Tong, *J. Am. Chem. Soc.*, 2012, **134**, 5730-5733.
16. Y. Wang, F. F. Shi, Y. Y. Yang and W. B. Cai, *J. Power Sources*, 2013, **243**, 369-373.
17. S. Y. Shen, T. S. Zhao, J. B. Xu and Y. S. Li, *J. Power Sources*, 2010, **195**, 1001-1006.
18. Z. Zhang, L. Xin, K. Sun and W. Li, *Int. J. Hydrogen Energy*, 2011, **36**, 12686-12697.

19. K. Lee, S.W. Kang, S.U. Lee, K.H. Park, Y.W. Lee, S.W. Han, *ACS Appl. Mater. Interfaces* 2012, **4**, 4208-4214.

